


# Large-Scale Crop Mapping From Multisource Remote Sensing Images in Google Earth Engine

Xinkai Liu, Han Zhai, Yonglin Shen , Benke Lou, Changmin Jiang, Tianqi Li, Sayed Bilal Hussain, and Guoling Shen

**Abstract**—Large-scale crop mapping is vitally important to agricultural monitoring and management. However, traditional methods cannot well meet the needs of large-scale applications. Therefore, this study proposed a method for large-scale crop mapping based on multisource remote sensing images. To be specific, 1) harmonic analysis was conducted on normalized difference vegetation index time-series derived from moderate resolution imaging spectroradiometer images and synthetic aperture radar backscattering coefficient time-series derived from Sentinel-1 data, respectively, extracting harmonic-derived phenological features and harmonic-derived backscattering features, and then combined with spectral features from Landsat-8 and Sentinel-2 images to construct the final multisource feature set for crop classification; 2) it employed prior constraints of crop dominance and cropland distribution to reduce misclassifications in large scale crop mapping; and 3) the whole process was conducted on the Google Earth Engine online platform, which can reduce the computational burdens caused by the spatiotemporal data. In the experimental study, we evaluated three crops, including wheat, rapeseed, and corn in Qinhai in 2018, based on the classification and regression tree classifier. The results show that the Jeffries–Matusita distances between crop samples are close to 2, and the overall accuracy is 84.25%. Furthermore, this study found that the distribution of the crops in Qinghai is associated with climate, topography, and cultivation habits.

**Index Terms**—Large-scale crop mapping, harmonic analysis, multisource feature set construction, multisource remote sensing images, prior constraints.

## I. INTRODUCTION

ACCURATELY and efficiently mapping the major crops is a prerequisite for precision agriculture, such as crop condition monitoring, phenology detection, yield prediction,

and disaster reduction, and is of great significance for macroeconomics, food security, agricultural policy-making, and environmental protection [1]. Currently, with the rapid development of earth observing techniques, abundant remote sensing images with high spatial and temporal resolutions are available [2], [3], which provide opportunities for comprehensive agricultural studies over longer time-spans based on multisource remote sensing data. However, in practical applications, traditional classification methods encounter many problems. Typically, due to different imaging mechanisms, temporal–spatial resolutions and various interferences, it is difficult to obtain multisource feature sets of high quality [4]. Especially for large-scale (regularly larger than a whole province) and long-term time-span (covering the whole crop growth season with high temporal resolution) crop mapping, the complex distribution of crops and insufficient training samples may lead to serious misclassification. In addition, the spatio-temporal datasets dramatically increase the cost of data storing and processing.

In the process of crop mapping, multisource feature set construction is a vitally important preliminary work, which directly affects the final mapping accuracy [5]. At present, many studies have been conducted on crop mapping with various features based on different remote sensing data. For example, Pacheco and McNairn [6] estimated percent crop residue cover with multispectral images based on spectral unmixing, with the root mean square errors being 17.29% and 20.74%, respectively. Satalino *et al.* [7] utilized C-band synthetic aperture radar (SAR) to map dominated/nondominated agricultural crops in Flevoland Netherlands by volume scattering. They used time-series of Radarsat-2 images to assess the performance of their algorithms, with the mean accuracy ranging from 75% to 90%. Baghdadi *et al.* [8] pointed out that SAR data are valuable in sugarcane crop monitoring by comparing different multitemporal SAR data. Boltion and Friedl [9] developed an empirical model to predict the distribution of corn and soybean using moderate resolution imaging spectroradiometer (MODIS) data and concluded that crop phenology metrics could be of significant benefit for corn and soybean yield predicting. In recent years, with the refined resolution of the spatiotemporal data and the improvement of classifiers, the accuracy of crop identification is being improved continuously [10]–[13]. However, crop mapping based on multispectral images tends to be seriously affected by weather conditions, and is often complicated by the problems of different objects with similar spectral signatures. In addition, they can hardly predict short-term crop progress stages. SAR has the advantage

Manuscript received July 17, 2019; revised October 27, 2019 and December 1, 2019; accepted December 16, 2019. Date of publication January 21, 2020; date of current version February 12, 2020. This work was supported by a grant from State Key Laboratory of Resources and Environmental Information System, Institute of Geographic Sciences and Natural Resources Research, Chinese Academy of Sciences (NO. 2018004), and in part by the National Natural Science Foundation of China under Grant 41501459 and Grant 41771380. (Corresponding author: Yonglin Shen.)

X. Liu, H. Zhai, B. Lou, C. Jiang, T. Li, S. B. Hussain, and G. Shen are with the School of Geography and Information Engineering, China University of Geosciences, Wuhan 430074, China (e-mail: liuxk@cug.edu.cn; zhaihhan@whu.edu.cn; 17673150918@163.com; 20141000446@cug.edu.cn; 809852709@qq.com; fakhriicup@yahoo.com; shen2529536@qq.com).

Y. Shen is with the School of Geography and Information Engineering, China University of Geosciences, Wuhan 430074, China, and also with the State Key Laboratory of Resources and Environmental Information System, Institute of Geographic Sciences and Natural Resources Research, Chinese Academy of Sciences, Beijing 100101, China (e-mail: shenyl@cug.edu.cn).

Digital Object Identifier 10.1109/JSTARS.2019.2963539

of all-day and all-weather monitoring, and verification of the effectiveness of SAR backscattering with different wavelengths and polarization modes in crop classification [14]–[16]. Blaes *et al.* [17] compared optical imagery and SAR data and pointed out that optical imagery has a dominant contribution to mapping accuracy, and SAR data are capable of further improving the accuracy to a higher level (more than 5%). On the other hand, classification based on normalized difference vegetation index (NDVI) time-series can be effectively enhanced by the phenological characteristics of the crop [18]–[21]. A common strategy is to extract phenological characteristics from the time-series of images with high-temporal resolution data (e.g., MODIS) [22]–[24]. The phenological characteristics are helpful to improve the classification accuracy. Some studies have shown that these features are possible to improve the sensitivity to the phenology evolution [25]. Moreover, the revisit period of many sensors such as Landsat (16 days) is too long to reflect the growth of many crops. Multisource feature sets can effectively overcome this issue by combining the advantages of multiple data sources. Integrating multiple datasets may also bring some compounding errors. Therefore, further imperative studies should be focused on the construction of multisource feature set with spectral, backscattering, and phenological characteristics.

Misclassifications are inevitable because of various uncertainties such as similar spectral and backscattering characteristics. In addition, the data noise (induced by cloud, observational condition, and calibration uncertainties) may also influence the classification accuracy [26]. The characteristics of cropland and woodland are very similar, especially when crops are around the heading date (when the leaves are luxuriant). Some small buildings are perpetually covered by trees, or they are close to cropland, so the misclassifications among cropland, building, and woodland are likely to occur. Furthermore, bare soil is easily confused with cropland and woodland as well, because fallow cropland and sparse woodland are similar to bare soil [27]. In crop classification, the following factors might lead to some errors to the classification result, such as the local cultivation habits, which may propagate errors in agricultural production monitoring or crop acreage calculation [28]. Unfortunately, traditional evaluation criteria do not provide any information regarding the spatial variability in classification [29]. Previous studies have shown that using the cropland boundaries can effectively reduce the classification errors due to the within-field spectral variability and mixed-pixels on the boundaries [30], [31].

Faced with the above problems in crop mapping, in this study, we proposed a method for large-scale crop mapping based on multisource remote sensing images. First, the harmonic analysis [32] is utilized to decompose NDVI time-series and SAR backscattering coefficient time-series with the obtained harmonic parameters to extract the phenological features and backscattering features, which can well describe the key characterizations of different crops. Then, these features are combined with the spectral features extracted from Landsat 8 Operational Land Imager (OLI) and Sentinel-2 Multispectral Instrument (MSI) multispectral signals to construct the final multisource feature set for crop classification. Finally, some prior constraints

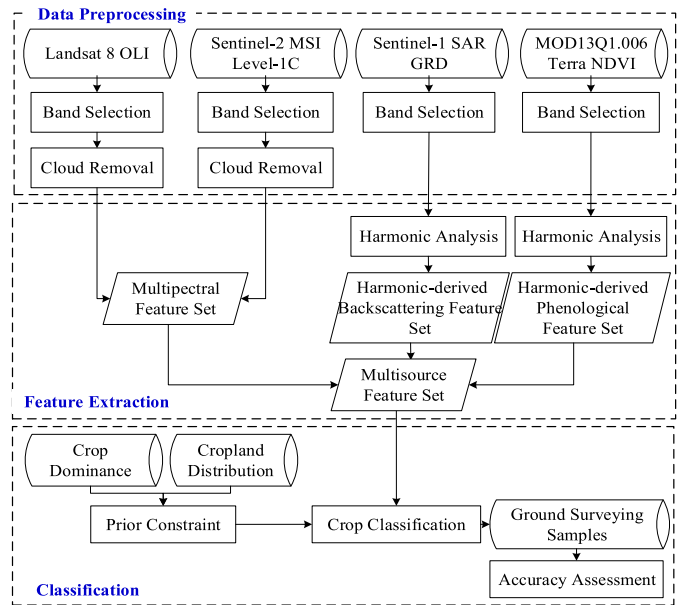


Fig. 1. Flow diagram of large-scale crop mapping.

of crop dominance and cropland distribution were employed to reduce misclassifications in large-scale crop mapping including Cropland Extent 1 km Crop Dominance, Global Food Security-support Analysis Data (GFSAD) (GFSAD1000) and GFSAD’s Cropland Extent 30 m (GFSAD30) which have been proved to be effective [33]. The whole process is based on the Google Earth Engine (GEE) to reduce the computational burdens caused by the massive spatiotemporal data, with the classification and regression tree (CART) tool utilized for crop classification. Finally, the proposed method is employed to evaluate the major three crops, wheat, rapeseed, and corn in Qinghai Province in 2018.

## II. MATERIALS AND METHODS

For the purpose of large-scale crop mapping, a strategy was put forward, as shown in Fig. 1. After necessary image preprocessing, harmonic analysis was employed to extract phenological features from NDVI time-series and backscattering features from SAR backscattering coefficient time-series; then, combined with spectral features from multispectral signals to construct multisource feature set; then, separability analysis of the constructed feature set was evaluated; finally, large-scale crop mapping was conducted with prior constraints in GEE platform.

It should be emphasized that GEE provides an efficient platform for the processing of massive multisource remote sensing data. It is a cloud-based platform for planetary-scale geospatial analysis that brings Google’s massive computational capabilities to address a variety of high-impact societal issues [34]. Because this platform supports online processing and computing for various remote sensing data, which overcomes the inefficiency problem associated with the large volumes of data, it has been widely used in many remote sensing applications [35]–[37].

TABLE I  
DESCRIPTIONS OF THE PRIMARY AND DERIVED REMOTE SENSING DATA USED IN THIS STUDY

NO.	Product	Sensor	Spatial Resolution	Temporal Resolution	Bands	Purpose
1	MOD13Q1 Vegetation Indices	MODIS Terra	250 m	16 days	NDVI	phenological feature set extraction
2	Landsat 8 Surface Reflectance	Landsat OLI	30 m	16 days	B2, B3, B4, B5, B6, B7	spectral features extraction
3	Sentinel-2 MSI Level-1C	Sentinel-2 MSI	20 m	5 days	B5	red-edge band
4	Sentinel-1 SAR GRD	Sentinel-1 SAR	10 m	3 days	VV+VH	backscattering features extraction
5	GFSAD1000	remote sensing derivatives	1 km	--	--	crop dominance
6	GFSAD30	remote sensing derivatives	30 m	--	--	cropland distribution

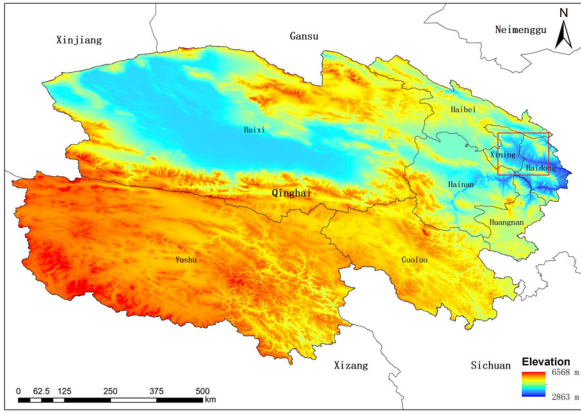


Fig. 2. Study area, and the color reflects the elevation change.

### A. Study Area and Datasets

Qinghai Province, which is adjacent to Xinjiang, Sichuan, Gansu, and Tibet, is located in the west of China and the north-east of the Qinghai-Tibet Plateau (see Fig. 2). Its geographic coordinates in the longitude ranges from  $89^{\circ}35'E$  to  $103^{\circ}04'E$ , and in the latitude ranges from  $31^{\circ}39'N$  to  $39^{\circ}19'N$ . The province covers an area of  $721\,200\text{ km}^2$ , accounting for 7.5% of the country's total area [38]–[40]. The three crops in this study include corn, wheat, and rapeseed. According to the observations of agrometeorological stations in Qinghai Province, the local crops are cultivated during a single growing season, which is mainly from March to October. The general sowing date of wheat is no earlier than March, the mature stage is in late August and early September, and the average growth period is about 140 to 170 days; the general sowing date of rapeseed is from March to April, the mature stage is from August to September, and the average growth period lasts for about 140 days; the general sowing date of corn is in April, its milky ripe stage comes in late September, and the harvest stage is around October. The remote sensing data we used cover from March 1 to October 31. This time-span covers the whole growth periods of the crops for harmonic analysis.

A variety of primary and derived remote sensing data were used in this study, which involved multispectral imagery (i.e., MODIS, Landsat 8, and Sentinel-2), SAR data (i.e., Sentinel-1)

and other ancillary grid data (i.e., crop dominance and cropland distribution). All data except cropland distribution are free and open-access in GEE platform; detailed descriptions are shown in Table I.

- 1) MODIS NDVI time-series, MODIS/Terra Vegetation Indices 16-Day L3 Global 250 m SIN Grid (MOD13Q1) product, with a spatial resolution of 250 m and temporal resolution of 16 days, was mainly used for crop phenological feature extraction.
- 2) Landsat 8 OLI, consists of nine spectral bands, with a spatial resolution of 30 m and temporal resolution of 16 days. B2 to B7 bands of Landsat-8 OLI were selected for this study.
- 3) Sentinel-2 MSI provides images with high spatial, spectral and temporal resolutions and incorporates two new spectral bands in the red-edge region. In particular, the “red-edge band” is especially useful for distinguishing the difference of different crops from foliar chlorophyll and canopy nitrogen [41]. Previous studies pointed out that the red-edge band in Sentinel-2 images, B5 (705 nm) band responds better to chlorophyll than B6 (740 nm) and B7 (783 nm) [42]. Therefore, B5 band of Sentinel-2, whose spatial resolution is 20 m and temporal resolution is 5 days, was used in this study.
- 4) Sentinel-1 dual-polarization C-band SAR instrument provides three resolutions (10, 25, and 40 m), four band combinations (corresponding to scene polarization) and three instrument modes.
- 5) Crop dominance is derived from the Cropland Extent 1 km Crop Dominance, GFSAD. It provides the spatial distribution of the major global cropland types (e.g., wheat, rice, corn, barley, and soybeans) by overlaying these crops over the remote sensing derived global irrigated and rainfed cropland area.
- 6) Cropland distribution is derived from the GFSAD's Cropland Extent 30 m. The data present the cropland distribution across the world in a nominal 30 m spatial resolution derived primarily with Landsat images, and they are available via the website (<https://web.croplands.org/app/map>).

Other data this study referred to include the administrative boundary vector, and ground surveying sample data of major crops in Qinghai Province, 2018. Among them, the ground



surveying sample data are obtained by field location-survey, which is used for classifier training, and accuracy assessment.

GEE provides various remote sensing products with different levels and a user interface to facilitate the preprocessing. Thus, the following data preprocessing was conducted by programming in GEE. MODIS NDVI time-series, Landsat 8 OLI, and Sentinel-2 MSI used in this study were atmospherically corrected by GEE. Each product provides quality bands for cloud removal. We adopted the temporal compression process on Landsat-8 and Sentinel-2 images separately to highlight the average progress stages during the entire growth period, which involved computing the median value of each pixel of selected multispectral signals within the time span from March 1 to October 31 in GEE. Sentinel-1 SAR GRD has been precorrected by GEE, including GRD border noise removal, thermal noise removal, radiometric calibration, and terrain correction. It should be pointed out that harmonic analysis has been proven to be an effective denoising method for time-series data [43], so the noise in NDVI time-series and SAR backscattering coefficient time-series can be ignored. In addition, in order to unify the spatial resolution and meet the requirements of subsequent classification algorithms, the multisource remote sensing data were resampled to 30 m.

### B. Harmonic Analysis on Multisource Time-Series

Decomposing the time-series  $Y$  into finite cosine (harmonic) waves superposition is the basic principle of harmonic analysis [44]. The data sequence consisting of these cosinoidal waves superposition is called the Fourier sequence ( $\hat{Y}$ ), and the mathematical expression is as follows:

$$y_i = A_0 + \sum_{j=1}^m A_j \cos(k_j i + \theta_j) \quad (1)$$

where  $A_0$  represents the harmonic remainder;  $A_j$  is the amplitude of each harmonic;  $\theta_j$  represents the initial phase of each harmonic;  $i = 1, 2, \dots, n$ , where  $n$  is the number of points of the fitted data;  $m$  is the number of harmonics; and  $k_j$  represents the harmonic frequency. The formula is as follows:

$$y_i = a_0 + \sum_{j=1}^m (a_j \sin k_j i + b_j \sin k_j i) \quad (2)$$

where  $a_0$  is the harmonic residual;  $a_j$  and  $b_j$  are the Fourier coefficients, which are calculated by linear fitting in this study, and other parameters that reflect the characteristics of the time-series (such as  $A_j$  and  $\theta_j$ ) are computed by these Fourier coefficients.

Fig. 3 illustrates the diagram of harmonic analysis on time-series. The reconstructed curve can preserve the trend of the original data and is much smoother and easier to describe. Meanwhile, the decomposed harmonic waves, which can be computed by Fourier coefficients, contain most information of the reconstructed curve. Therefore, these Fourier coefficients obtained by harmonic analysis can represent the characteristics of time-series to a certain extent, which is proven to be an effective approach for data dimensionality reduction [45]. The figure also reveals that first three harmonics after decomposition contain most information that is capable of describing the growth change of crops. To

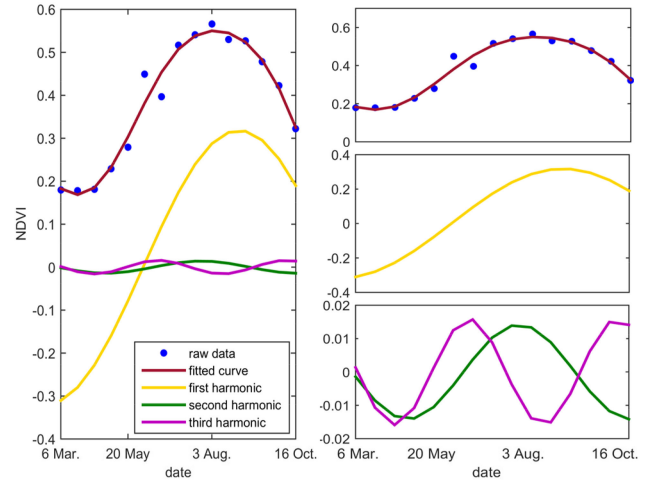


Fig. 3. Diagram of harmonic analysis on time-series.

be specific, the first harmonic can reflect the overall trend of the whole curve, so its amplitude  $A_1$  is an indicator to describe the undulation of the curve, while initial phase  $\theta_1$  carries some temporal information that expresses the date when the peak appears. The second and third harmonics are related to the details of the curve. When curve is smooth, the intensity of the fluctuation of the second and third harmonic is weak, and the values of  $A_2$  and  $A_3$  are small. When the local details of crop growth are revealed in the curve, which makes the curve fluctuate obviously, the corresponding  $A_2$  and  $A_3$  to the second and third harmonics increase as well. In summary, the following parameters are estimated.

- 1)  $A_0$ : is harmonic residual, which represents the average value of the curve.
- 2)  $y_{\max}$ : is the maximum value in the fitted data set  $Y_{fit}$ , which can be used to indicate the peak value of the curve.
- 3)  $\theta_1$ : is the initial phase of the first harmonic, which is used to indicate the temporal discrepancies of the maximum value.
- 4)  $A_1$ : is the amplitude of the first harmonic, which is used to indicate the overall trend of the curve.
- 5)  $A_{flu} = A_2 + A_3$ : is the sum of the amplitudes of the second harmonic ( $A_2$ ) and third harmonic ( $A_3$ ), which is used to characterize the details of the curve.

### C. Feature Extraction and Feature Set Construction

As previously mentioned, spectral, backscattering, and phenological features have both advantages and disadvantages for crop mapping. Comprehensively using multisource feature set is significantly valuable in enhancing the separability of different kinds of crops and improving the classification accuracy. However, due to different imaging mechanisms of different data types and diverse factors impacting the quality of data, the multisource feature set may contain compounded uncertainties. For example, multispectral data are susceptible to weather conditions, which inevitably leads to noise or data missing in time-series. Backscattering coefficients are likely to be affected by various factors, such as crop growth environment, and the

variation characteristics of backscattering time-series are not easy to generalize. Therefore, it is imperative to design effective feature extraction and multisource feature set construction flow for larger scale and longer term situations. Therefore, in this study, phenological features and backscattering features were extracted utilizing harmonic analysis, and then combined with spectral features to construct a multisource feature set.

1) *Harmonic-Derived Phenological Feature Extraction:* Phenology is the study of the timing of recurring biological events, the causes of changes concerning biotic and abiotic forces, and the interrelation among phases of the same or different species [46]. Different crops have unique phenological characteristics, which can be detected from NDVI time-series. The obtained Fourier sequence  $a_j$  and  $b_j$  of harmonic analysis can be used to compute the phenological features, revealing the crop growth implicit in the NDVI profile [47]. To be specific, harmonic analysis of NDVI time-series is valuable in describing changes of the start-of-season, end-of-season, duration, and fluctuation of the crop phenology [48].

The harmonic residual  $A_0$  represents the temporal signal or the average value in half-cycle of the sequence, so this indicator represents the average value of the NDVI profile in a crop growth period, which can reflect the productivity of the crop to a certain extent; the amplitude  $A_j$  represents the fluctuation intensity of each harmonic, so the amplitude superposition of harmonics can represent the fluctuation of the NDVI profile; the phase  $\theta_j$  mathematically represents the displacement of the harmonic peak relative to the origin point. Considering phenological characteristics of a given crop, this parameter can indicate the date of NDVI peak appearing, reflecting the temporal variation of the maximum greenness and coverage of different crops. MOD13Q1 NDVI data were used to conduct harmonic analysis and phenological features extraction.

2) *Harmonic-Derived Backscattering Feature Extraction:* SAR backscattering coefficient contains information related to vegetation growth. Therefore, its time-series can be used to evaluate crop growth and changes of crops, especially given that as they are available in all weather conditions [14], [17]. Thus, it is reasonable to extract backscattering features through the change of backscattering coefficient in the time-series [49], [50]. These temporal changes are helpful in enhancing the characterizations of the crops and improving mapping accuracy.

In this study, we used harmonic analysis to extract backscattering features from SAR backscattering coefficient time-series. Similarly to the NDVI time-series analysis, we selected harmonic residual  $A'_0$ , maximum value  $y'_{\max}$ , initial phase  $\theta'_1$ , the first harmonic  $A'_1$  and  $A'_{\text{fly}} = A'_2 + A'_3$  as harmonic-derived backscattering features. Furthermore, we selected two linear polarizations (VV and VH) within the study area. It must be pointed out that the complexity of the scattering mechanisms of crops might make the analysis of temporal curves more difficult [51], and the potential uncertainty caused by this may impact the accuracy of the classification. As for data preprocessing, besides selecting temporal duration and spatial extension, the modes were filtered to reduce data heterogeneity; only “wide interference”/“derailment observation” data were selected.

3) *Multisource Feature Set Construction:* In addition to phenological features and backscattering features, we also combined the spectral features from Landsat-8 and Sentinel-2 multispectral signals to construct a multisource feature set. Based on the above methods of feature extraction, the dimension of the final multisource feature set for crop classification in this study is 22, including five phenological features, ten backscattering features, and seven spectral features. Phenological features, as indicators for the dynamic progress of crops, can be very useful in improving the separability of different crop types [52]. Backscattering features have advantages in eliminating the impacts of weather factors to a certain extent compared with optical sensors. The multisource feature set in this study takes advantage of all three types of features (i.e., phenological, backscattering, and spectral) into account.

Compared with other methods of feature set construction, this method has advantages in overcoming inconsistencies among different datasets in the process of large-scale feature extraction, and it is able to minimize the uncertainties of features and summarize crop growth changes. Furthermore, if the weights of different types of features in the constructed dataset are significantly different, the classification results will be dependent on the features with higher weights. In this study, after construction, the dimensions of the three types of features are nearly the same, which resulted in relatively equal contributions from each feature type in the final classification.

#### D. Separability Evaluation of Feature Set

To evaluate the effectiveness of the constructed feature set for crop classification, separability analysis was performed on the extracted features for different crops. Separability indices commonly used include divergence, transform separability, Bhattacharyya distance, and Jeffries–Matusita (JM), in which JM distance is considered to be more suitable for indicating the separability between classes than other indices [53]. The mathematical expression of the JM distance is formulated as follows:

$$J = 2 \cdot (1 - e^{-B}) \quad (3)$$

where  $B$  is the Bhattacharyya distance on a certain feature dimension. The formula for calculating the Bhattacharyya distance between two different classes whose probability density functions  $p_1(x)$  and  $p_2(x)$  conform to random distribution is as follows:

$$B = -\ln \left( \int \sqrt{p_1(x)p_2(x)} dx \right). \quad (4)$$

Assuming that these sample classes distributed as the normal distribution,  $B$  distance can be expressed as follows:

$$B = \frac{1}{8}(m_1 - m_2)^2 \frac{2}{\delta_1^2 + \delta_2^2} + \frac{1}{2} \ln \left[ \frac{\delta_1^2 + \delta_2^2}{2\delta_1\delta_2} \right] \quad (5)$$

where  $m_i$  represents the mean of feature value of a specific class;  $\delta_i^2$  is the variance,  $i = 1, 2$ . The range of JM distance is [0, 2], 0 means that the two categories are completely confused, and 2 means that the two categories can be completely separated [54]. Then, the separability of the four crop types (wheat, corn, rapeseed, and “other”) are evaluated by the JM distance.

### E. Crop Classification With Prior Constraints

This study used the CART classifier to conduct crop classification, which has been integrated into the GEE platform. CART is a decision tree construction algorithm proposed by Breiman [55]. It is based on subsequent binary splits of a dependent variable according to cut-off values or classes of independent variables [56]. The CART algorithm uses the Gini Index in economics as the criterion for selecting the best variable [57]. Its mathematical expression is as follows:

$$\text{Gini Index} = 1 - \sum_j P^2(j/h), \quad (6)$$

$$P(j/h) = \frac{n_j(h)}{n(h)}, \sum_j P(j/h) = 1 \quad (7)$$

where  $P(j/h)$  indicates the probability that the testing variable  $h$  belongs to the  $j$ th class when the sample is randomly selected in the sample set;  $n_j(h)$  is the number of samples in which the testing variables  $h$  belong to the  $j$ th class;  $n(h)$  is the total number of the training samples in which the testing variables are  $h$ ; and  $j$  is the class number. CART algorithm selects one or more attributes from a plurality of input attributes as splitting variables, then assigns testing variables to branches. We repeated the processing to establish a classification tree and selected the optimal classification tree through pruning and testing. The feature set was first normalized by mean and variance, then the classification process was conducted and results/confusion matrices exported.

The purpose of adding prior constraints to the classification process is to control the spatial extent of classification. It is based on the assumption that the crops distribute within the cropland extent. However, the conventional evaluation methods only focus on the classification accuracy based on testing samples and ignore the discrepancies between classification results and real cropland distribution, which will influence the practical application of these methods. To solve this problem, this study developed a classification method with prior constraints. The advantages of the prior constraints are: 1) the prior constraint can control the distribution of the crop type of the classification result. When the classification result has a significant deviation from the distribution indicated by the prior constraint, the result is in a high probability deviating from the local cultivation habits; and 2) the prior constraint controls the spatial extent of the classification, reducing the probability of noncrop objects participating in the classification, some training samples away from where the crop concentrating are also eliminated. A global food support analysis product published by USGS, GDFAD1000, records the spatial distribution of the major crops, and GS-FAD30 records the cropland distribution around the world, which are suitable to be used as the prior constraints. In this study, we overlapped the two products within the study area to generate a mask to produce images with only those areas laid in the overlapped area selected.

## III. RESULTS AND DISCUSSIONS

In order to verify the effectiveness of the proposed method on large-scale crop mapping, the separability of the feature set

was analyzed and classification accuracy was evaluated. Additionally, crop characteristics and spatial distribution in Qinghai Province are discussed.

In the separability analysis of the feature set, pure pixels (those that are in the middle of the cropland and are not affected by non-crop objects) were selected from the ground surveying samples of the crops and plotted to compare different features to analyze the differences; then evaluated the separability of the feature set by calculating the JM distances between the samples. In this study, the proposed full-feature set, which combines spectral features, harmonic-derived backscattering features, and harmonic-derived phenological features, was compared with the following five features, including spectral features; compressed backscattering features; harmonic-derived backscattering features; harmonic-derived phenological features; combination of spectral features and harmonic-derived backscattering features. The compressed backscattering feature went through the process of compression, which was similar to that of spectral feature, computing the mean of the backscattering coefficient in each pixel during the whole growth period.

In the comparative experiments of classification, we evaluated the multisource feature set through the overall accuracy (OA) of classification results. When conducting the hold-out accuracy assessment, 70% of the ground samples were selected for training and the remaining for testing. We set six comparative experiments to verify the influence of feature extraction on classification accuracy:

- 1) using spectral features with prior constraints, hereafter, MC;
- 2) using compressed backscattering features with prior constraints, hereafter, CC;
- 3) using harmonic-derived backscattering features with prior constraints, hereafter, BC;
- 4) using the combination of harmonic-derived phenological features with prior constraints, hereafter, PC;
- 5) using the combination of spectral features and harmonic-derived backscattering features with prior constraints, hereafter, MBC;
- 6) using the combination of spectral features, harmonic-derived backscattering features and harmonic-derived phenological features without prior constraints, hereafter, MBP.

The method proposed in this study, which uses the combination of spectral features, harmonic-derived backscattering features, and harmonic-derived phenological features with prior constraints, is abbreviated as MBPC.

### A. Separability Analysis of Feature Set

The samples that the JM distance analyses conducted on are pure pixels selected from the ground surveying samples. Therefore, they are relatively less affected by noise, and the results can better reflect the separability of the feature set. As shown in Table II, it is clear that except for compressed backscattering features, all cases of features show good separability. The distances of spectral features are all larger than 1.5, and the distances between corn and rapeseed, corn and "other," rapeseed and "other" even exceed 1.9, indicating strong separability.



TABLE II  
DISTANCE BETWEEN SAMPLES

NO.	Feature		Corn	Wheat	Rapeseed	Others
1	spectral features	Corn		1.7584	1.9556	1.9526
		Wheat	1.7584		1.7833	1.5475
		Rapeseed	1.9556	1.7833		1.9246
		Others	1.9526	1.5475	1.9246	
2	compressed backscattering features	Corn		0.4798	0.1263	0.2410
		Wheat	0.4798		0.6543	0.6215
		Rapeseed	0.1263	0.6543		0.2007
		Others	0.2410	0.6215	0.2007	
3	harmonic-derived backscattering features	Corn		1.3794	1.8257	1.6223
		Wheat	1.3794		1.7707	1.7366
		Rapeseed	1.8257	1.7707		1.6259
		Others	1.6223	1.7366	1.6259	
4	harmonic-derived phenological features	Corn		1.7207	1.7600	1.6379
		Wheat	1.7207		1.5325	1.1596
		Rapeseed	1.7600	1.5325		1.4038
		Others	1.6379	1.1596	1.4038	
5	combination of spectral features and harmonic-derived backscattering features	Corn		1.9864	1.9997	1.9998
		Wheat	1.9864		1.9987	1.9948
		Rapeseed	1.9997	1.9987		1.9988
		Others	1.9998	1.9948	1.9988	
6	full-feature set	Corn		1.9999	2.0000	2.0000
		Wheat	1.9999		2.0000	1.9998
		Rapeseed	2.0000	2.0000		2.0000
		Others	2.0000	1.9998	2.0000	

The JM distances of compressed backscattering features are all less than 0.7, which means the separability is very poor. For harmonic-derived backscattering features, the distance between wheat and corn is 1.3794, and the rest exceed 1.6. This indicates that the backscattering based on harmonic analysis effectively enhances the separability of the samples. The distances of the harmonic-derived phenological features are generally around 1.5, only the distance between wheat and “other” types is 1.1596.

The JM distances of combined feature sets are further compared with the single-source features, indicating that multi-source feature sets have considerable potential for improving classification accuracy. When the spectral features are combined with harmonic-derived backscattering features, the JM distances are larger than 1.98, which means the feature set has great separability. The distances of the full-feature set are very close to 2, meaning the samples can be completely separated. It is concluded that the full-feature set constructed in this study can effectively enhance the separability of crops for classification.

### B. Comparison and Analysis of the Classification Results

The classification result of the whole Qinghai Province is shown in Fig. 4. Fig. 5 shows a close-up view of the northeastern area of Qinghai Province, and its spatial extent corresponds to the range of red boxes in Fig. 2. The confusion matrix and OA are shown in Table III.

1) *Spatial Distribution*: Fig. 4 shows the spatial distribution of classification results of the crops, i.e., corn, wheat, rapeseed, and “other classes.” It is clear that, after adopting the prior constraints, the spatial distribution of the major crops classified by the classifier is consistent with the local cultivation

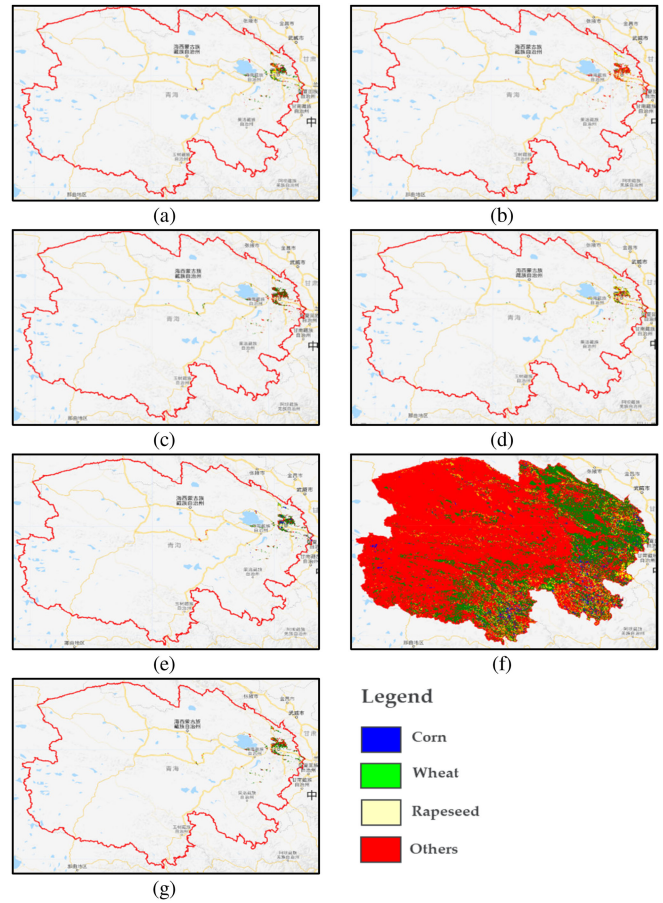


Fig. 4. Spatial distribution of classification results of the whole Qinghai Province, (a) to (g) are MC, CC, BC, PC, MBC, MBP, and MBPC, respectively.

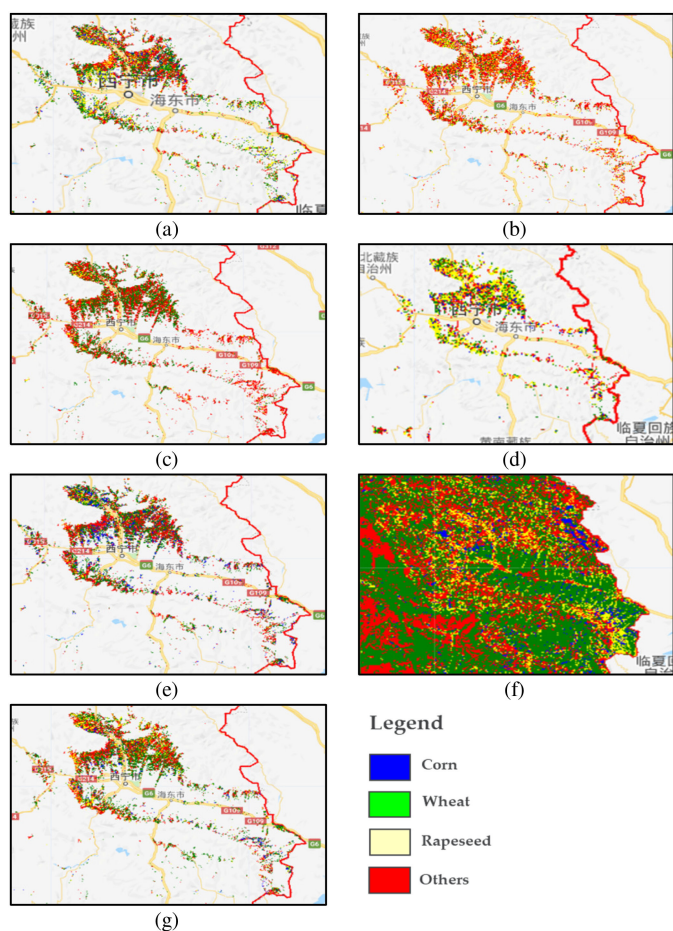


Fig. 5. Crop distribution in major agricultural region and valley region of Qinghai Province. (a) to (g) are MC, CC, BC, PC, MBC, MBP, and MBPC, respectively.

habits. As major crops in Qinghai Province, the three crops are distributed around the east to Qinghai Lake and southwest to Qilian Mountain, where the local natural conditions are suitable for cultivation, this region is the major agricultural region. Furthermore, valleys which are situated southwest to Xining are also the main region where the crops are present. When the classification is conducted without prior constraints, the areas identified as the distribution of the crops are much larger than the actual distribution, which is unrealistic [see Fig. 4(f)].

Fig. 5 reveals the detail of crop distribution in major agricultural region and valley region of Qinghai Province. For different combinations of features with prior constraints, the results are different. For MC [see Fig. 5(a)], it shows that the three crops are concentrated in the northern, southern, and western parts of the major agricultural region, and there is also large distribution in the valley region. The rapeseeds are concentrated in the southern part of the major agricultural region and the northern part of the valley region, and the cultivated area of corn in the central part of the major agricultural region is relatively larger than other regions. MC responded poorly to corn samples, the planning area of corn is small in the classification result. SAR data are severely noisy and its influencing factors are complex, thus the data processed by temporal compression is unable to reflect the

distribution correctly. It can be seen from Fig. 5(b), for CC, most of the study area is identified as “other classes,” the crops are only sporadically distributed in the major agricultural region. The classification result of BC is better than that of CC. However, as described previously, the characteristics of SAR backscattering coefficient time-series of crops are still complicated. The mixed distribution of various crops is still obvious in the classification result.

In Fig. 5(c), large areas are identified as wheat, and rapeseed in the north, while the response of BC to corn is still poor. As for the result of PC [see Fig. 5(d)], it is more likely to identify the samples as rapeseed. In the figure, rapeseeds are mainly distributed in the northern part of the major agricultural region and the valley region, and the cultivated area is large and concentrated. Corn and wheat are mainly distributed in the northern and central parts of the major agricultural region, which are relatively mixed. Furthermore, large areas of the central and southern major agricultural regions are identified as other types of crops. The spatial distribution of the classification result of MBC is similar to that of MC, while the cultivated area of corn and wheat is relatively larger. For MBPC, the three crops are also concentrated in the northern, central, and southern parts of the major agricultural region, and they are distributed in the valley region as well. Among them, rapeseeds are mainly distributed in the northern and western parts of the major agricultural region and in the northern part of the valley. The corn is mainly distributed in the central part of the major agricultural region, and the southern part is dominated by wheat. The distribution of the three crops is scattered in general.

2) *Quantitative Comparative Analysis*: The accuracies of different classification strategies are shown in Table III. The OA of MC is 78.67%, and the Kappa coefficient is 0.6867. It can be seen from the confusion matrix that the accuracy of corn is higher, and the separability between wheat, rape and “others” is slightly worse. The misclassification between wheat and “others” is relatively higher (4.43% testing samples of wheat are misclassified into “others” and 3.57% testing samples of “others” are misclassified into “wheat”). The OA of CC is only 58.36%, and the Kappa coefficient is 0.3643, which is almost valueless. Meanwhile, The OA of BC was improved compared to CC, reaching 64.71%, and the Kappa coefficient is 0.4727. The accuracy of the crops increases with 1.04 for corn, 2.6 for wheat, and 3.97 for rapeseed. Only the accuracy of the “other” decreases with 1.26. Considering the previous analysis, it is concluded that backscattering features based on harmonic analysis effectively enhances the separability of samples and has considerable potential to improve the accuracy of crop identification compared to conventional methods. Phenological features are capable of predicting crop progress stages, which is a good indicator of the accurate identification of crops. From the classification results, the OA of harmonic-derived phenological features is the highest among all single-source features, which is 81.52%, and the Kappa coefficient is 0.7268. Among the crops, only 2.41% testing samples of wheat were misclassified into rapeseed, whose value is larger than 1%. It is noticeable that compared with BC, when the backscattering features are combined with the spectral features (MBC), the OA is slightly improved to 79.08%,



TABLE III  
CLASSIFICATION ACCURACY FOR DIFFERENT METHODS AND DIFFERENT CROPS

NO.	Methods	Confusion Matrix (%)				OA (%)	Kappa	
		Corn <sup>1</sup>	Wheat	Rapeseed	Others			
1	MC <sup>3</sup>	Corn <sup>2</sup>	4.20	0.95	0.77	1.13	78.67	0.6867
		Wheat	0.72	11.70	1.36	3.57		
		Rapeseed	0.32	2.26	30.73	3.30		
		Others	1.27	4.43	1.27	32.04		
2	CC <sup>4</sup>	Corn	0.55	0.51	1.33	4.73	58.36	0.3643
		Wheat	0.41	4.73	6.11	5.93		
		Rapeseed	0.83	3.68	24.63	7.12		
		Others	0.92	3.86	6.20	28.45		
3	BC <sup>5</sup>	Corn	1.59	1.87	0.59	3.60	64.71	0.4727
		Wheat	0.55	7.33	3.23	5.24		
		Rapeseed	0.50	1.68	28.60	4.46		
		Others	2.05	5.60	5.92	27.19		
4	PC <sup>6</sup>	Corn	4.25	0.72	0.87	1.45	81.52	0.7268
		Wheat	0.04	12.54	0.72	3.14		
		Rapeseed	0.10	2.41	33.00	1.54		
		Others	1.78	2.07	3.62	31.74		
5	MBC <sup>7</sup>	Corn	4.80	0.83	0.28	0.97	79.08	0.6902
		Wheat	1.11	9.75	1.43	4.02		
		Rapeseed	0.51	1.57	32.15	3.00		
		Others	1.71	3.37	2.12	32.38		
6	MBP <sup>8</sup>	Corn	3.89	0.79	0.51	1.14	81.73	0.7341
		Wheat	0.76	15.61	2.53	1.14		
		Rapeseed	0.54	1.58	32.33	2.34		
		Others	0.95	2.62	2.37	29.90		
7	MBPC <sup>9</sup>	Corn	4.32	0.65	0.28	0.88	84.25	0.7651
		Wheat	0.65	12.12	2.28	2.37		
		Rapeseed	0.23	1.16	31.40	1.90		
		Others	0.93	2.93	1.49	36.41		

<sup>1</sup>Ground truth of *in situ* survey; <sup>2</sup>classified results; <sup>3</sup>spectral features with prior constraints; <sup>4</sup>compressed backscattering features with prior constraints; <sup>5</sup>harmonic-derived backscattering features with prior constraints; <sup>6</sup>harmonic-derived phenological features with prior constraints; <sup>7</sup>combination of spectral features and harmonic-derived backscattering features with prior constraints; <sup>8</sup>combination of spectral features, harmonic-derived backscattering features and harmonic-derived phenological features without prior constraints; <sup>9</sup>combination of spectral features, harmonic-derived backscattering features and harmonic-derived phenological features with prior constraints.

indicating that the harmonic-derived backscattering features are significant for enhancing the separability of spectral features.

The classification by using constructed full-feature set and prior constraints in this study (i.e., MBPC) obtains the best accuracy, the OA reaches 84.25%, and the Kappa coefficient is 0.7651. It overcomes the defects of all the single-source features at the same time. Moreover, when the prior constraints are unconsidered, some sample data in poor quality are brought for classifier training, which leads to a decrease in classification result. The OA of MBP drops to 81.73%. It proves the necessity of using prior constraints of crop dominance and cropland distribution for crop classification. It should also be pointed out that in this study, the training samples of “others” can from different ground object types, which seriously influences the separability. From Table III, it is clear that the misclassification between “others” and specific crop types are mostly heavier than those between crops. Taking MC as example, the misclassification between “others” and crops are all larger than 1%, there are even 4.43% of the pixels in testing which belong to wheat are misclassified to “others.” Similar phenomenon also appears in other features.

From the results of separability analysis and classification experiments, it can be concluded that the comprehensive utilization of the multisource feature set is better than only

utilizing single-source features. By containing the information on crop characteristics, environmental changes, and manual management, the phenological features can provide abundant information. The backscattering features can make up for the obstacles of spectral features, such as data missing and noise. Compared with the traditional feature extraction method, the proposed method takes into account the characteristics of different sources of features to compensate for the deficiencies of single-source features. The reconstructed multisource feature set is more separable and more recapitulative, which reduces the uncertainty of time-series and highlights its overall trend of crop growth. From the experimental results, it can be found that the proposed method can obtain the best classification accuracy. Moreover, the prior constraints are added in the classification process to control the spatial range, and eliminate the unreliable training data to further improve the accuracy of crop mapping.

### C. Crop Mapping Analysis

The multisource remote sensing data used in this study for crop mapping spans the whole growth season of the selected crops, and the spatial extent of the study area is the Qinghai Province, the spatial resolution after resampling is 30 m. From the experimental results, it is concluded that the fitting curves

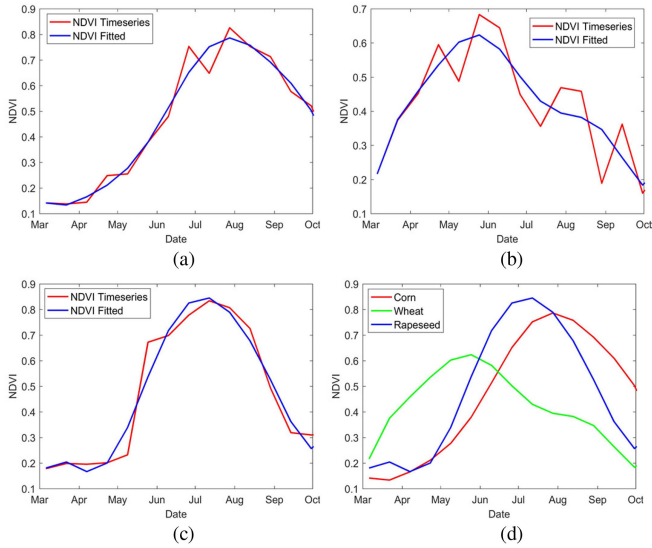


Fig. 6. NDVI time-series of (a) corn, (b) wheat, and (c) rapeseed and (d) their comparison of fitted data.

themselves are important for analyzing the growth trends of local crops, and the distribution of the crops in the experimental result is consistent with local farming habits. Therefore, it is valuable for us to analyze the factors impacting local farming habits.

1) *Characteristics of Crops*: The NDVI time-series of the selected crops in growing period shows unimodal trends. It is consistent with the growth changes recorded by agrometeorological stations that the crops have only one growing season per annum. The geometric characteristics, the maximum value, and the time when the key phenological stages appear in the NDVI profile are significantly different [58], [59]. In Fig. 6(a), the entire growth period of corn lasts from the end of March to October. The growing rate keeps increasing during the seeding stage; after that, the growing rate remains stable. In middle and late July, the NDVI curve reaches the maximum, which is about 0.8, then the NDVI gradually decreases after the crops enter maturity; the sowing date of wheat is the earliest among the crops, the growing period is the longest, and the maximum of the NDVI curve is the smallest (only about 0.6). In Fig. 6(b), the sowing date is in March, and the growing rate increases obviously during the seeding stage, then the growing rate decreases a bit. The NDVI curve reaches peak in the end of June, then values start decreasing. In mid-July, the crops enter maturity; by contrast, the growing period of rapeseed is shorter, the duration of growth and maturity is shorter as well. In Fig. 6(c), the rapeseeds are sown in mid-to-late April, and the seeding stage is in May. The florescence is in mid-to-late June, which is followed by reaching maximum in July, the value is about 0.85. Then, NDVI begins to decline and crops gradually enter maturity.

The harmonic analysis also has a good effect on restoring the temporal characteristics of the backscattering coefficient curves. In Fig. 7, the fitting backscattering coefficient curves after harmonic analysis eliminate the influences of noise well, and the curve is smoother. In general, the temporal characteristics of crop backscattering features are more complicated,

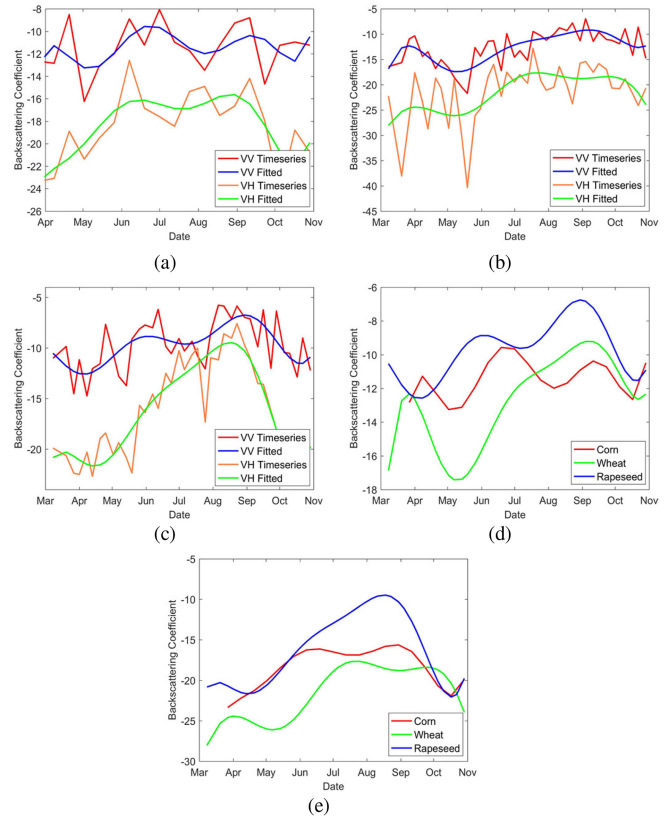


Fig. 7. SAR time-series of corn (a), wheat (b) and rapeseed (c) and their comparison of fitted data [VV is shown in (d) and VH is in (e)].

and the uncertainty is more serious. For crop identification, the cross-polarized band was found to be more sensitive to crop growth than the co-polarized band [50]. VH polarization has a better response to crop growth changes than VV, and the characteristics of VH are more prominent. The change of the backscattering coefficient curves has correlations with the growth of the crops [60].

Specifically, in Fig. 7(a), the curve of VV of corn is relatively flat. There are three smaller peaks in the seeding stage in early April, the elongation stage in mid-June and the mid-September which is in maturity. The VH polarization curve is relatively steep. The backscattering coefficient increases before the elongation stage, then the first peak appeared in early June, followed by a slight decrease. The second peak appeared at the end of August, and then continued to decrease as crops enter maturity; the curve of wheat is stable, and the trend of the two polarization modes of VV and VH are same. In Fig. 7(b), small peaks appear in the seedling stage in the middle and late March, and then the backscattering coefficient slowly increases. The curve keeps stable until maturity in September, when the backscattering coefficient begins to decrease; it is interesting that there were significant differences in the VV and VH curves of rapeseed. In Fig. 7(c), the first peak of VV curve appears in mid-May, then decreasing a little bit as the result of the increasing of plant height and density. The crops enter maturity in late August, when the variation of canopy increases and reflecting signal the sensor receiving enhances, where the second

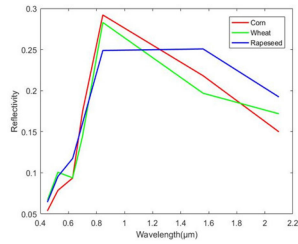


Fig. 8. Comparison of spectral features of corn, wheat, and rapeseed.

peak appears in the curve. By contrast, the VH curve shows unimodal characteristic, and the backscattering coefficient continues to increase before the maturity period, then it drops dramatically. Furthermore, it can be seen from the figures that the backscatter coefficient curves of the crop confront serious noise effects, so the uncertainty of the backscattering features is much heavier.

Fig. 8 shows the spectral signatures of the three crops from Landsat-8 OLI and Sentinel-2 MSI sensors. In general, the typical “square root” shape of the crops is consistent overall. It is noticeable that the reflectivity of corn and wheat in every band is relatively close. As a result, it shows that the effect of crop identification with single-phase multispectral data is limited to some extent. Specifically, the red band has a higher reflectivity for rapeseed, and the reflectivity for corn and wheat in that band is very similar. The reflectivity of rapeseed is lower in near-infrared (NIR) band (850–880 nm) and higher in two short wave infrared (SWIR) bands (1.57–1.65 and 2.11–2.29 nm). In contrast, the trend of reflectivity of wheat in NIR and SWIR bands is similar to that of corn while the reflectance value is lower.

#### 2) Characteristics of Crop Distribution in Qinghai Province:

From the experimental results, the spatial distribution of the local crops in Qinghai is relatively complicated and fragmented. This distribution characteristic is mainly caused by various natural and human conditions such as topographic conditions, climates, and the small-holder agricultural production. As the result, the crop classification is susceptible to the spectral variability and impure training sample. Therefore, it is necessary to improve the classification accuracy with prior constraints of crop dominance and cropland distribution.

The spatial distribution of crops is related to the terrain of Qinghai Province. For cropland distribution, the major agricultural region is located in south of Daban Mountain, which is the branch of Qilian Mountain, and east of Riyue Mountain. This area is the overlaid zone of the Loess Plateau to Qinghai-Tibet Plateau. Our experimental result also shows that the terrain of this area is rugged, and the croplands are distributed mostly along the rivers and valleys. Therefore, the distribution of croplands is relatively fragmented, which is not conducive to large scale centralized agriculture. Furthermore, the local agricultural economic structure is dominated by small scale peasant economy, the process of agricultural industrialization is lagging behind, and agricultural production is still carried out mainly by families or collectives, making the types of crop complicated and the cultivated acreage of a certain type of crop small.

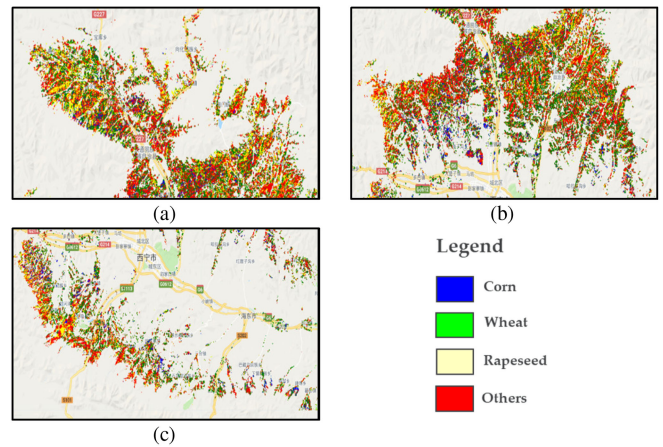


Fig. 9. Local maps of eastern major agricultural region in Qinghai, (a) is the northern part, (b) is the middle part, and (c) is the southern valleys.

The climatic conditions are the most important factors affecting the distribution of crops. In the northern and northeastern parts of the major agricultural region [shown in Fig. 9(a)], mainly covering the valleys of Datong County and Huzhu County, the climate is warm and humid, with an annual average precipitation of 400 mm or more, the warmest monthly average temperature of  $\sim 11.5\text{--}13.5\text{ }^{\circ}\text{C}$  and the accumulated temperature (AT, an indicator reflecting local thermal conditions [61]) of  $\sim 1500\text{--}2000\text{ }^{\circ}\text{C}$ . The water conditions are abundant but the thermal conditions are common, so the chimonophilous crops such as rapeseed are concentrated in the colder area. In central part [see Fig. 9(b)], covering north of Xining, the climate is characterized as warm and semi-arid, where the annual average temperature is above  $3\text{ }^{\circ}\text{C}$ , the warmest monthly average temperature is higher than  $15\text{ }^{\circ}\text{C}$ , and AT is  $\sim 2000\text{--}3000\text{ }^{\circ}\text{C}$ . The thermal conditions in this area are better, but the precipitation is relatively poor, the average precipitation is less than 400 mm. Thus, the type of cultivation in this area is mainly irrigation agriculture. The climate conditions can meet the requirements of spring wheat, rapeseed, and other crops’ cultivation. The result of our classification shows that the distribution of wheat in this area is concentrated, and there is a small amount of corn distribution in the south of this area. Although the southern valley area [see Fig. 9(c)] is small, the climatic conditions are the best. In some areas, the annual average temperature is above  $19\text{ }^{\circ}\text{C}$ , and the AT is over  $3500\text{ }^{\circ}\text{C}$ . The annual average precipitation is relatively low, below 360 mm, but concentrated in the crop growing season. Meanwhile, as the result of many rivers flowing through this area, the irrigation conditions in this area are good. Therefore, the area is suitable for a variety of crop growth, and yields are higher. It can be seen from the experimental results that there are a large number of distributions of the three selected crops in the area. Overall, the classification results of this study reflect the local crop cultivation habits.

#### IV. CONCLUSION

For large-scale crop mapping, with the increasing temporal and spatial resolution of remote sensing images, traditional data



processing and analyzing methods are confronted with several challenges, such as unstable multisource feature sets, serious misclassification, and large computational complexity, which greatly limits the practical ability of these methods in crop mapping at large scale. Therefore, this study proposed a new crop mapping method with prior constrains and used the proposed method for three main crops classification in Qinghai in 2018. Compared with the classification results from single-source features, we found that the classification accuracy of multisource feature set is considerably better, and the proposed feature extraction method performs well in eliminating noise and restoring the temporal trend. The JM distance between the samples is close to 2, and the OA is 84.25%, which means that the proposed method is effective in enhancing separability and improving the classification accuracy. The prior constraints can effectively control the classification area and eliminate some training samples of low quality, so it can reduce the misclassification to some degree. Finally, the GEE platform is helpful to improve computing efficiency and make large-scale crop mapping more practical. The multisource feature set construction and crop mapping method proposed in this study has a high application value in crop mapping in a complex terrain and crop distribution environment. It is able to provide aid for many fields such as agricultural management, yield prediction, and environmental monitoring.

#### ACKNOWLEDGMENT

The authors would like to thank Prof. P. Lewis from the Department of Geography at University College London, who provided general advice on the review. Acknowledgement for “The 1st Smart Agricultural Remote Sensing Application Competition of Sentinels of Wheat” sponsored by China Agricultural University, University College London, and Chinese Academy of Agricultural Sciences.

#### REFERENCES

- [1] M. Ozdogan, “The spatial distribution of crop types from MODIS data: Temporal unmixing using independent component analysis,” *Remote Sens. Environ.*, vol. 114, pp. 1190–1204, 2010.
- [2] Z. Chen *et al.*, “Progress and perspectives on agricultural remote sensing research and applications in China,” *J. Remote Sens.*, vol. 748–767, 2016.
- [3] M. Wang, “Comparison of spatial interpolation and regression analysis models for an estimation of monthly near surface air temperature in China,” *Remote Sens.*, vol. 9, 2017, Art. no. 1278.
- [4] Z. Liu and W. Zong, “Image classification optimization algorithm based on SVM,” *J. Multimedia*, vol. 8, pp. 496–502, 2013.
- [5] Q. Zou, L. Ni, T. Zhang, and Q. Wang, “Deep learning based feature selection for remote sensing scene classification,” *IEEE Geosci. Remote Sens. Lett.*, vol. 12, no. 11, pp. 2321–2325, Nov. 2015.
- [6] A. Pacheco and H. McNairn, “Evaluating multispectral remote sensing and spectral unmixing analysis for crop residue mapping,” *Remote Sens. Environ.*, vol. 114, pp. 2219–2228, 2010.
- [7] G. Satalino, A. Balenzano, F. Mattia, and M. Davidson, “Sentinel-1 SAR data for mapping agricultural crops not dominated by volume scattering,” in *Proc. IEEE Int. Geosci. Remote Sens. Symp.*, 2012, pp. 6801–6804.
- [8] N. Baghdadi, N. Boyer, P. Todoroff, M. E. Hajj, and A. Bégué, “Potential of SAR sensors TerraSAR-X, ASAR/ENVISAT and PALSAR/ALOS for monitoring sugarcane crops on reunion island,” *Remote Sens. Environ.*, vol. 113, pp. 1724–1738, 2009.
- [9] D. K. Bolton and M. Friedl, “Forecasting crop yield using remotely sensed vegetation indices and crop phenology metrics,” *Agricultural Forest Meteorol.*, vol. 173, pp. 74–84, 2013.
- [10] A. Mathur and G. M. Foody, “Crop classification by support vector machine with intelligently selected training data for an operational application,” *Int. J. Remote Sens.*, vol. 29, pp. 2227–2240, 2008.
- [11] P. Hao, W. Li, and N. Zheng, “Potential of multitemporal Gaofen-1 panchromatic/multispectral images for crop classification: Case study in Xinjiang Uygur Autonomous Region, China,” *J. Appl. Remote Sens.*, vol. 9, 2015, Art. no. 096035.
- [12] C. Yang, J. H. Everitt, and D. Murden, “Evaluating high resolution SPOT 5 satellite imagery for crop identification,” *Comput. Electron. Agriculture*, vol. 75, pp. 347–354, 2011.
- [13] P. Upadhyay, A. Kumar, P. S. Roy, S. K. Ghosh, and I. Gilbert, “Effect on specific crop mapping using WorldView-2 multispectral add-on bands: Soft classification approach,” *J. Appl. Remote Sens.*, vol. 6, 2012, Art. no. 063524.
- [14] H. Skriver, “Crop classification by multitemporal C- and L-band single and dual-polarization and fully polarimetric SAR,” *IEEE Trans. Geosci. Remote Sens.*, vol. 50, no. 6, pp. 2138–2149, Jun. 2012.
- [15] K. Jia, Q. Li, Y. Tian, B. Wu, F. Zhang, and J. Meng, “Crop classification using multi-configuration SAR data in the North China Plain,” *Int. J. Remote Sens.*, vol. 33, pp. 170–183, 2012.
- [16] H. Skriver *et al.*, “Crop classification using short-revisit multitemporal SAR data,” *IEEE J. Sel. Topics Appl. Earth Observ. Remote Sens.*, vol. 4, no. 2, pp. 423–431, Jun. 2011.
- [17] X. Blaes, L. Vanhalle, and P. Defourny, “Efficiency of crop identification based on optical and SAR image time series,” *Remote Sens. Environ.*, vol. 96, pp. 352–365, 2005.
- [18] D. Bargiel, “A new method for crop classification combining time series of radar images and crop phenology information,” *Remote Sens. Environ.*, vol. 198, pp. 369–383, 2017.
- [19] S. Hariharan, D. Mandal, S. Tirodkar, V. Kumar, A. Bhattacharya, and J. M. Lopez-Sanchez, “A novel phenology based feature subset selection technique using random forest for multitemporal PolSAR crop classification,” *IEEE J. Sel. Topics Appl. Earth Observ. Remote Sens.*, vol. 11, no. 11, pp. 4244–4258, Nov. 2018.
- [20] M. Boschetti, “PhenoRice: A method for automatic extraction of spatio-temporal information on rice crops using satellite data time series,” *Remote Sens. Environ.*, vol. 194, pp. 347–365, 2017.
- [21] Y. Pan, L. E. Li, J. Zhang, S. Liang, X. Zhu, and D. Sulla-Menashe, “Winter wheat area estimation from MODIS-EVI time series data using the crop proportion phenology index,” *Remote Sens. Environ.*, vol. 119, pp. 232–242, 2012.
- [22] B. D. Wardlow, S. L. Egbert, and J. H. Kastens, “Analysis of time-series MODIS 250 m vegetation index data for crop classification in the U.S. Central Great Plains,” *Remote Sens. Environ.*, vol. 108, pp. 290–310, 2007.
- [23] C. Conrad, R. R. Colditz, S. Dech, D. Klein, and P. L. G. Vlek, “Temporal segmentation of MODIS time series for improving crop classification in Central Asian irrigation systems,” *Int. J. Remote Sens.*, vol. 32, pp. 8763–8778, 2011.
- [24] P. Hao, Y. Zhan, W. Li, N. Zheng, and M. Shakir, “Feature selection of time series MODIS data for early crop classification using random forest: A case study in Kansas, USA,” *Remote Sens.*, vol. 7, pp. 5347–5369, 2015.
- [25] C. D. Bernardis, F. Vicente-Guijalba, T. Martinez-Marin, and J. M. Lopez-Sanchez, “Contribution to real-time estimation of crop phenological states in a dynamical framework based on NDVI time series: Data fusion with SAR and temperature,” *IEEE J. Sel. Topics Appl. Earth Observ. Remote Sens.*, vol. 9, no. 8, pp. 3512–3523, Aug. 2016.
- [26] Z. Wu, L. Yi, and G. Zhang, “Uncertainty analysis of object location in multi-source remote sensing imagery classification,” *Int. J. Remote Sens.*, vol. 30, pp. 5473–5487, 2009.
- [27] L. Ma, L. Cheng, M. Li, Y. Liu, and X. Ma, “Training set size, scale, and features in geographic object-based image analysis of very high resolution unmanned aerial vehicle imagery,” *ISPRS J. Photogrammetry Remote Sens.*, vol. 102, pp. 14–27, 2015.
- [28] F. Löw, P. Knöfel, and C. Conrad, “Analysis of uncertainty in multi-temporal object-based classification,” *ISPRS J. Photogrammetry Remote Sens.*, vol. 105, pp. 91–106, 2015.
- [29] L. Loosvelt *et al.*, “Random Forests as a tool for estimating uncertainty at pixel-level in SAR image classification,” *Int. J. Appl. Earth Observ. Geoinf.*, vol. 19, pp. 173–184, 2012.
- [30] A. J. W. De Wit and J. G. P. W. Clevers, “Efficiency and accuracy of per-field classification for operational crop mapping,” *Int. J. Remote Sens.*, vol. 25, pp. 4091–4122, 2004.
- [31] M. Turker and M. Arıkan, “Sequential masking classification of multi-temporal Landsat7 ETM+ images for field-based crop mapping in Karabey, Turkey,” *Int. J. Remote Sens.*, vol. 26, pp. 3813–3830, 2005.

- [32] J. Zhou, J. Li, and M. Menenti, "Reconstruction of global MODIS NDVI time series: Performance of harmonic analysis of time series (HANTS)," *Remote Sens. Environ.*, vol. 163, pp. 217–228, 2015.
- [33] K. Yadav and R. G. Congalton, "Accuracy assessment of global food security-support analysis data (GFSAD) cropland extent maps produced at three different spatial resolutions," *Remote Sens.*, vol. 10, 2018, Art. no. 1800.
- [34] N. Gorelick, M. Hancher, M. Dixon, S. Ilyushchenko, D. Thau, and R. Moore, "Google earth engine: Planetary-scale geospatial analysis for everyone," *Remote Sens. Environ.*, vol. 202, pp. 18–27, 2017.
- [35] J. Dong *et al.*, "Mapping paddy rice planting area in northeastern Asia with Landsat 8 images, phenology-based algorithm and Google Earth Engine," *Remote Sens. Environ.*, vol. 185, pp. 142–154, 2016.
- [36] D. Mandal, V. Kumar, A. Bhattacharya, Y. S. Rao, P. Siqueira, and S. Bera, "Sen4Rice: A processing chain for differentiating early and late transplanted rice using time-series Sentinel-1 SAR data with Google Earth Engine," *IEEE Geosci. Remote Sens. Lett.*, vol. 15, no. 12, pp. 1947–1951, Dec. 2018.
- [37] A. Shelestov, M. Lavreniuk, N. Kussul, A. Novikov, and S. Skakun, "Exploring Google Earth Engine platform for big data processing: Classification of multi-temporal satellite imagery for crop mapping," *Frontiers Earth Sci.*, vol. 5, pp. 1–10, 2017.
- [38] J. Zhao and J. Peng, "Spatiotemporal variation of the vegetation coverage in Qinghai Plateau based on MODIS NDVI data," *J. Arid Land Resources Environ.*, vol. 30, pp. 67–73, 2016.
- [39] L. Wang, Y. Wei, and Z. Niu, "Analysis of vegetation spatial and temporal variations in Qinghai Province based on remote sensing," *Environ. Sci.*, vol. 29, pp. 1754–1760, 2008.
- [40] P. Wu and X. Zhang, "Estimation methods of reference crop evapotranspiration in eastern agricultural region of Qinghai Province," *J. Irrigation Drainage*, vol. 34, pp. 97–101, 2015.
- [41] A. Ramoelo, A. K. Skidmore, M. A. Cho, M. Schlerf, R. Mathieu, and I. M. A. Heitkönig, "Regional estimation of savanna grass nitrogen using the red-edge band of the spaceborne RapidEye sensor," *Int. J. Appl. Earth Observ. Geoinf.*, vol. 19, pp. 151–162, 2012.
- [42] J. Ú. Delegido, J. Verrelst, L. Alonso, and J. É. Moreno, "Evaluation of sentinel-2 red-edge bands for empirical estimation of green LAI and chlorophyll content," *Sensors*, vol. 11, pp. 7063–7081, 2011.
- [43] Y. Gang, H. Shen, L. Zhang, Z. He, and X. Li, "A moving weighted harmonic analysis method for reconstructing high-quality spot vegetation NDVI time-series data," *IEEE Trans. Geosci. Remote Sens.*, vol. 53, no. 11, pp. 6008–6021, Nov. 2015.
- [44] R. De Jong, S. De Bruin, A. De Wit, M. E. Schaepman, and D. L. Dent, "Analysis of monotonic greening and browning trends from global NDVI time-series," *Remote Sens. Environ.*, vol. 115, pp. 692–702, 2011.
- [45] J. J. Benedetto and W. Czaja, "Dimension reduction and remote sensing using modern harmonic analysis," in *Handbook of Geomathematics*. Berlin, Germany: Springer, 2013, pp. 1–22.
- [46] D. Lloyd, "A phenological classification of terrestrial vegetation cover using shortwave vegetation index imagery," *Int. J. Remote Sens.*, vol. 11, pp. 2269–2279, 1990.
- [47] G. J. Roerink, M. H. G. I. Danes, O. G. Prieto, A. J. W. De Wit, and A. J. H. Van Vliet, "In deriving plant phenology from remote sensing," *Anal. Multi-Temporal Remote Sens. Images*, vol. 1, pp. 261–264, 2011.
- [48] L. Andres, W. A. Salas, and D. Skole, "Fourier analysis of multi-temporal AVHRR data applied to a land cover classification," *Int. J. Remote Sens.*, vol. 15, pp. 1115–1121, 1994.
- [49] H. Joerg, M. Pardini, I. Hajnsek, and K. Papathanassiou, "Sensitivity of SAR tomography to the phenological cycle of agricultural crops at X-, C- and L-band," *IEEE J. Sel. Topics Appl. Earth Observ. Remote Sens.*, vol. 11, no. 9, pp. 3014–3029, Sep. 2018.
- [50] H. Li, C. Zhang, S. Zhang, and P. M. Atkinson, "Full year crop monitoring and separability assessment with fully-polarimetric L-band UAVSAR: A case study in the Sacramento Valley, California," *Int. J. Appl. Earth Observ. Geoinf.*, vol. 74, pp. 45–46, 2018.
- [51] J. M. Lopez-Sanchez and J. D. Ballester-Berman, "Potentials of polarimetric SAR interferometry for agriculture monitoring," *Radio Sci.*, vol. 44, no. 2, pp. 1–20, Apr. 2009.
- [52] Y. Gu, J. F. Brown, T. Miura, W. J. D.V. Leeuwen, and B. C. Reed, "Phenological classification of the united states: A geographic framework for extending multi-sensor time-series data," *Remote Sens.*, vol. 2, pp. 526–544, 2010.
- [53] S. Ullah, T. A. Groen, M. Schlerf, A. K. Skidmore, W. Nieuwenhuis, and C. Vaiphasa, "Using a genetic algorithm as an optimal band selector in the mid and thermal infrared (2.5–14  $\mu\text{m}$ ) to discriminate vegetation species," *Sensors*, vol. 12, pp. 8755–8769, 2012.
- [54] A. M. O. Sousa, J. M. C. Pereira, and J. M. N. Silva, "Evaluating the performance of multitemporal image compositing algorithms for burned area analysis," *Int. J. Remote Sens.*, vol. 24, pp. 1219–1236, 2003.
- [55] L. Breiman, J. H. Friedman, R. A. Olshen, and C. J. Stone, *Classification and Regression Trees*. Boca Raton, FL, USA: Chapman & Hall/CRC, 1984.
- [56] S. D'Alisa, G. Miscio, S. Baudo, A. Simone, L. Tesio, and A. Mauro, "Depression is the main determinant of quality of life in multiple sclerosis: A classification-regression (CART) study," *Disability Rehabil.*, vol. 28, pp. 307–314, 2006.
- [57] L. Rutkowski, M. Jaworski, L. Pietruczuk, and P. Duda, "The cart decision tree for mining data streams," *Inf. Sci.*, vol. 266, pp. 1–15, 2014.
- [58] V. Chandola, D. Hui, L. Gu, B. Bhaduri, and R. R. Vatsavai, "In Using time series segmentation for deriving vegetation phenology indices from MODIS NDVI data," in *Proc. IEEE Int. Conf. Data Mining Workshops*, 2011, pp. 202–208.
- [59] S. Testa, K. Soudani, L. Boschetti, and E. B. Mondino, "MODIS-derived EVI, NDVI and WDRVI time series to estimate phenological metrics in French deciduous forests," *Int. J. Appl. Earth Observ. Geoinf.*, vol. 64, pp. 132–144, 2018.
- [60] F. Canisius *et al.*, "Tracking crop phenological development using multi-temporal polarimetric Radarsat-2 data," *Remote Sens. Environ.*, vol. 210, pp. 508–518, 2017.
- [61] S. H. Hallett and R. J. A. Jones, "Compilation of an accumulated temperature database for use in an environmental information system," *Agricultural Forest Meteorol.*, vol. 63, pp. 21–34, 1993.



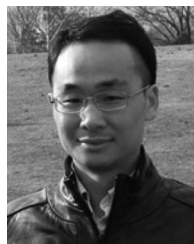
**Xinkai Liu** received the B.Sc. degree from the College of Information Science and Engineering, Shandong Agricultural University, Taian, China, in 2016. He is currently working toward the M.Sc. degree in remote sensing of environment and natural resources from China University of Geosciences.

His research interests include remote sensing applications in agriculture and vegetation.



**Han Zhai** received the B.Sc. degree from the School of Surveying and Mapping, Shandong University of Science and Technology, Qingdao, China, in 2014, and the Ph.D. degree from the State Key Laboratory of Information Engineering in Surveying, Mapping, and Remote Sensing, Wuhan University, Wuhan, China, in 2019.

He is an Associate Professor with the China University of Geosciences, Wuhan. His research interests include remote sensing image processing, remote sensing information extraction, and sparse representation.



**Yonglin Shen** received the B.Sc. degree in geography information system from the Wuhan University of Technology, Wuhan, China, in 2006, the M.Sc. degree from Nanjing Normal University, Nanjing, China, in 2009, and the Ph.D. degree from Beijing Normal University, Beijing, China, in 2013, both in cartography and geography information system.

During 2011–2013, he worked as a joint Ph.D. student with the Center for Spatial Information Science and Systems, George Mason University, Fairfax, VA, USA. He is currently an Associate Professor with the

China University of Geosciences, Wuhan. His research interests include remote sensing applications in agriculture and atmospheric environment.



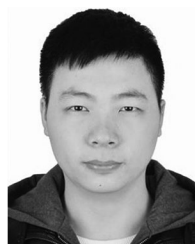
**Benke Lou** received the B.Sc. degree from the College of Central South University of Forestry and Technology, Changsha, China, in 2018. He is currently working toward the M.Sc. degree in surveying and mapping engineering from China University of Geosciences, Wuhan, China.



**Sayed Bilal Hussain** received the Bachelor of Computer Science degree from the University of Peshawar, Peshawar, Pakistan, in 2012. He is currently working toward the M.Sc. degree in software engineering from the China University of Geosciences, Wuhan, China.



**Changmin Jiang** received the B.Sc. degree from the School of Geography and Information Engineering, China University of Geosciences, Wuhan, China, in 2018. He is currently working toward the M.Sc. degree in surveying and mapping engineering from China University of Geosciences.



**Guoling Shen** received the B.Sc. degree from the School of Geography and Information Engineering, China University of Geosciences, Wuhan, China, in 2019. He is currently working toward the M.Sc. degree in remote sensing of environment and natural resources from the China University of Geosciences.



**Tianqi Li** received the B.Sc. degree from the School of Geography and Information Engineering, China University of Geosciences, Wuhan, China, in 2019. She is currently working toward the M.Sc. degree in remote sensing of environment and natural resources from China University of Geosciences.